Confinement, surface, and chemisorption effects on the optical properties of Si quantum wires

Chin-Yu Yeh, S. B. Zhang, and Alex Zunger
National Renewable Energy Laboratory, Golden, Colorado 80401
(Received 15 July 1994)

We have used the empirical pseudopotential method to study the electronic and optical properties of [001] Si quantum wires with (110)-($\bar{1}$10) square cross sections ranging from 4×4 to 14×14 monolayers (7.7×7.7 to 26.9×26.9 Å, respectively). We present energy levels, band gaps, oscillator-strength, and charge-density distributions. To understand the electronic structure of these systems we calculate their properties in a stepwise process, considering (1) wires with a free surface but without hydrogen and (2) wires with hydrogen chemisorption on the surface. We find that (i) in both cases, the band gap between bulklike states increases as the wire size is reduced (due to quantum confinement). However, (ii) hydrogen chemisorption acts to reduce the gap. (iii) Whereas the low-energy states near the valence-band *minimum* are effective-mass-like, the near-band-gap states with or without H on the surface can be decisively non-effective-mass-like. The lowest conduction states are pseudodirect, not direct. (iv) The calculated energy dependence of the transition lifetimes is too strong to explain the observed low-energy "slow" emission band in porous Si purely in terms of transitions in an ideal wire. However, an alternative model, which introduces a mixture of wires and boxes, can account for the experimental slope.

I. INTRODUCTION

Since Si has an *indirect* band gap (1.13 eV), pristine Si has poor optical radiative efficiency at threshold. Despite this, recent experimental observations[1,2] on porous Si have shown that Si quantum wires exhibit strong visible photoluminescence (PL) around 1.6 to 2.5 eV at room temperature with a size-dependent peak position. These observations have stimulated intense experimental activity in this field.[2] Of particular interest here is the physical origin of the intense, blueshifted emission.

Recent room temperature time-resolved PL experiments have found two different emission bands:[3–5] the low-energy S band and the high energy F band (Fig. 1). The low-energy S band peaks in the deep red[5] (1.72 eV), has a half width of 0.3–0.4 eV (Ref. 4), and a stretched-exponential type of decay with a lifetime that depends on the emission energy. Its integrated intensity accounts for 97% of the red emission from conventional porous silicon with an overall room-temperature lifetime of $\sim 3\times10^{-5}$ sec (Ref. 5). This emission vanishes as the material is oxidized above 700 °C (Ref. 6) or if it is heavily hydrogenated by immersing in HF under UV light.[4] The quenching of the emission is often accompanied by the emergence of a strong spin signal, suggesting that dangling bonds are implicated in the quenching of the PL. Since conventional porous Si is not monodispersed but has instead a broad distribution of wire widths (e.g., 30±10 Å in Ref. 5) and a variety of different shapes, a single sample can emit over a broad energy range. Examining the lifetimes at different emission energies shows that these could be fitted by assuming two decay channels with an energy difference in the range of 10–30 meV [see Fig. 2(c) in Ref. 5]. The upper level lifetime is around 5 μsec ("slow"), and the lifetime of the lower level is around 3 msec ("very slow").

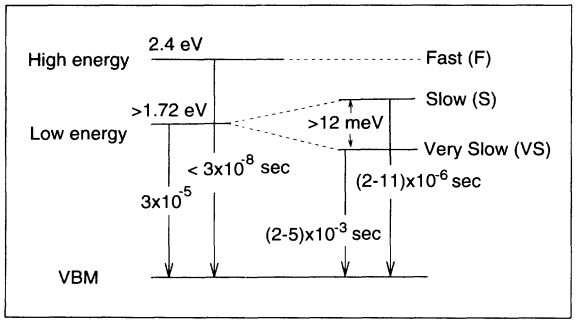

FIG. 1. Schematic depiction of the main emission peaks and lifetimes observed by Calcott *et al.* (Ref. 5) for anodically prepared porous Si. Data for τ_{slow}, $\tau_{very\ slow}$ and "exchange" splitting are from Ref. 5.

The high-energy F band peaks at the green-blue[5] (2.4 eV), has a half width of ~0.3 eV, and a decay time faster than 3×10^{-8} sec. It accounts for only 1–3% of the emission in conventional porous silicon. It is unaffected[4] by oxidation (up to 700 °C) or by immersion in HF: since it exists in oxihydride, oxide, and pure hydride samples, it was suggested that this emission represents the *intrinsic* properties of the Si skeleton rather than the chemisorption layer, and that this emission can be enhanced by reducing the particle size.

In the present paper we focus on the following questions regarding Si quantum wires: (a) what causes the blueshift? — is it a quantum confinement effect or a surface effect? (b) what causes the intense PL and (c) what are the origins of the main emitting states of Fig. 1?

Previous calculations[7–11] suggested that the blueshift of the emission relative to bulk Si is likely to represent a quantum size effect. However, it is not clear if the *intensity* and *lifetimes* can be explained just in these terms: Most calculations show that the conduction-band minimum of the wire is made largely from bulk Δ_c states[7,8,10] so the band gap of the wire is *pseudodirect*, not direct. This leads to rather small transition probabilities and long lifetimes. Coupling to other bands and to surface states (most prominent in small wires) induces some finite oscillator strength, shortening thereby the radiative lifetime from infinity. A number of calculations attempted to establish if the pseudodirect transition is strong enough to explain the observed radiative lifetime, in terms of quantum confinement. The calculations of Hybertsen and Needels[11] considered wires whose width is much narrower than experiment, so their calculated lifetimes cannot be directly compared with experiment. Read *et al.*[7] calculated $\tau_R = 3.8 \times 10^{-4}$ sec for a 9×8 structure in reasonable agreement with the measured $\tau_R = 6.5 \times 10^{-5}$ sec at E_g=1.7 eV. However, Read *et al.* did not calculate τ_R vs wire size. Here, we will calculate the matrix elements and radiative lifetimes extending the wire sizes to the measurable range. As will be shown below, we find that the calculated τ_R rises with increasing size (decreasing band gap) much faster than the observed τ_R. Thus uniform-wire models, which include nonparabolic bands, multiband coupling, and surface effects, *cannot* by themselves explain the observed energy dependence of the transition lifetime of the slow band. We show, however, that these observations are consistent with a picture of a wire-dot mixture.

Another issue we want to address is the significance of surface chemisorption effects. Previous theoretical work on this subject[7,8,10] considered Si wires covered with H atoms. Here we are interested in the *isolation* of hydrogen chemisorption effects. We first perform direct supercell calculation on wires with a free surface but without hydrogen. Only transitions between bulklike states in the wires are considered. In the second step, we perform direct supercell calculation on wires with hydrogen chemisorbed on the surface. The difference between the two steps provides information on hydrogen chemisorption effects. In both cases, we used the empirical pseudopotential methods (EPM) in a plane wave basis, which allow us to cover a wide range of wire sizes extending the range accessible to local density approximation (LDA) calculation. The EPM has certain advantages over the tight-binding scheme: it allows a detailed analysis at the wave functions; no explicit assumption on the boundary conditions is necessary. We have studied the effects of quantum confinement, surface chemisorption on the energy levels, band gaps, wave functions, decay lifetimes, and the oscillator strength of Si quantum wires with square cross sections ranging from 4×4 to 14×14 monolayers (7.7 × 7.7 to 26.9 × 26.9 Å, respectively). Section II describes the pseudopotential method used for direct pseudopotential calculations of wires with free surfaces and with hydrogen chemisorption. Section III describes an effective-mass approach (EMA) used for comparison and a wave-function projection scheme for analyzing results. Section IV summarizes all the present results, while Sec. V provides discussions and conclusions.

II. THE DIRECT HAMILTONIAN DIAGONALIZATION APPROACH

Here, we discuss the direct diagonalization approach to Si wires with a free surface [Fig. 2(a)] and, separately, covered with H [Fig. 2(b)]. In solving the Schroedinger equation,

$$(-\tfrac{1}{2}\nabla^2 + V^{\text{wire}})\psi^{\text{wire}}(\mathbf{r}) = \epsilon^{\text{wire}}\,\psi^{\text{wire}}(\mathbf{r}), \tag{1}$$

we construct $V^{\text{wire}}(\mathbf{r})$ from a superposition of atomic (Si and H) pseudopotentials. Figure 3(a) shows a cross section of the atomic geometry used for a wire along (001) with free surfaces (110)×(1$\bar{1}$0). In this case, there are dangling bonds on the wire surface, leading to surface states in the band gap. Using contour plots of the wave function, we identify these states. Since we are interested here in transitions between bulklike states in the wire, these surface states are discarded from the following discussion. Figure 3(b) shows a cross section of the atomic geometry used for the hydrogen-covered surface.

In all "direct calculations," we have used a supercell geometry by adding four atomic layer of vacuum around the wire and repeating the wire+vacuum unit cell periodically. The square wires have cross sections ranging from 4×4 to 14×14 monolayers (7.7 × 7.7 to 26.9 × 26.9 Å). The bond length used for Si-Si is 2.34 Å (the experimental bulk Si value[12]) whereas for Si-H we use 1.48 Å. The Si monolayer separation a_L along the [110] direction is 1.92 Å. Using these values, the length L of a bare 8×8 square wires is 15.36 Å.

We use a local empirical pseudopotential for Si of the following form:[13]

$$V(q) = b_1(q^2 - b_2)/(b_3 e^{b_4 q^2} - 1), \tag{2}$$

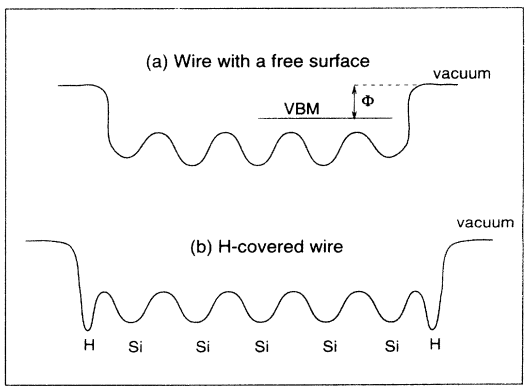

FIG. 2. Schematic diagrams showing the z-direction potential averaged over the x-y plane for (a) wire with free surface, and (b) hydrogen-covered wire. In part (a) Φ denotes the work function separating the valence-band maximum (VBM) from vacuum.

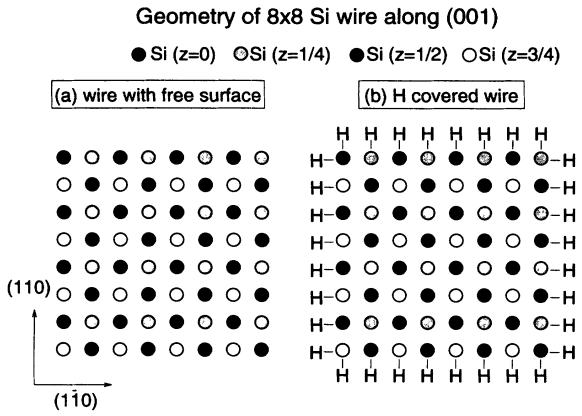

FIG. 3. Geometry of a (001)-oriented 8×8 Si wire with (110) × (1$\bar{1}$0) cross section, (a) free-surface wire and (b) hydrogen-covered wire.

where q is a continuous wave vector. The four parameters $\{b_i\}$ in Eq. (2) were determined by fitting the bulk band structure at Γ, X, and L,[14] and the experimental work function[15] of Si. Details were discussed in Ref. 13.

The hydrogen empirical pseudopotential used here was fitted to the observed surface density of state of hydrogen covered (001), (111), and (110) Si surfaces[16] (potential A). However, in order to test the sensitivity of the results to the H potential, we have also constructed a molecular H potential[17] (potential B) by fitting the energy levels of SiH_4 as calculated by Ellis *et al.*[18] An analogous molecular-type potential was used recently in tight-binding Si film calculated by Gavrilenko *et al.*[19] The energy levels obtained with these two H potentials for the 4×4 Si wire are shown in Fig. 4. In another calculation[16] on H-covered Si *surface*, it was found that the molecular potential (B) produces H antibonding conduction-band surface states that are ~1 eV too low compared to experimental data. In our *wire* calculation (viz. Fig. 4) we find that the molecular potential (B) gives a band gap smaller than potential A by 0.3 eV for a 4×4 wire, and 0.07 eV for a 12×12 wire. Furthermore, the molecular potential produces a doubly degenerate valence-band maximum (VBM), while the surface-fitted potential (A) produces a singly degenerate VBM. We use here potential A because we believe that it is appropriate to Si wires whose surfaces resemble those of semi-infinite crystals.

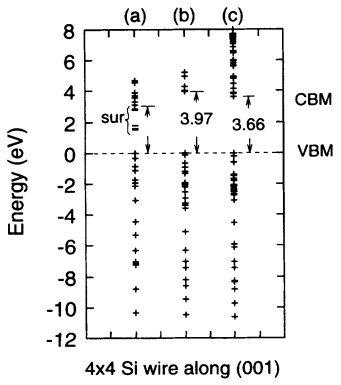

FIG. 4. Energy spectra of a Si 4 × 4 wire. (a) The free-surface wire. There are eight occupied surface ("sur") states in the band-gap region. (b) The H-covered wire using hydrogen potential A and (c) the H-covered wire using hydrogen potential B.

III. THE EFFECTIVE-MASS APPROACH AND WAVE-FUNCTION PROJECTIONS

A. Effective-mass approximation

It is useful to compare our results of direct calculation with the widely used EMA. In the EMA, the periodic potentials in Fig. 2 are renormalized away and the energy dispersions near energy extrema $\mathbf{k}=\mathbf{k}_0$ are replaced by

$$\epsilon_n^{\mathrm{EMA}}(\mathbf{k}) = \epsilon_{n,\mathbf{k}_0}^{\mathrm{bulk}} + \hbar^2\mathbf{k}^2/2m_n^* , \tag{3}$$

where n is the band index, $\mathbf{k}$ is the wave vector, and m_n^* is the effective mass. The wave functions of wires, in the simplest single band approximation, are approximated by products of a periodic bulk Bloch function $\mathrm{u}(\mathbf{r})$ at n, $\mathbf{k}=\mathbf{k}_0$ and an envelope function ϕ, i.e.,

$$\psi_{n,\mathbf{k}}^{\mathrm{EMA}} = u_{n,\mathbf{k}_0}(\mathbf{r})\phi_{\mathbf{k}}(\mathbf{r}). \tag{4}$$

Using a particle-in-a-box approach with boundary conditions, $\phi(0,y,z) = \phi(L,y,z) = \phi(x,0,z) = \phi(x,L,z) = 0$ for the envelope functions, one can solve the Schroedinger equation for ϕ which yields (1) a quantization of wave vector $\mathbf{k}$ into a set of discrete $\mathbf{k}^*$,

$$k_x^* = \frac{j_x\pi}{L}, \quad k_y^* = \frac{j_y\pi}{L}, \quad j_x, j_y = \text{positive integers}, \tag{5}$$

(2) a quantized energy spectrum,

$$\epsilon_n^{\mathrm{EMA}} = \epsilon_{n,\mathbf{k}_0}^{\mathrm{bulk}} + \frac{\hbar^2}{2m_n}(k_x^{*2} + k_y^{*2}), \tag{6}$$

and (3) an EMA wave function

$$\begin{aligned}\psi_n^{\mathrm{EMA}} &= Cu_{n,\mathbf{k}=\mathbf{0}}(\mathbf{r})\phi(k_x,k_y) \\ &= Nu_{n,\mathbf{k}=\mathbf{0}}(\mathbf{r})\sin(k_x^*x)\sin(k_y^*y),\end{aligned} \tag{7}$$

where C is a normalization constant.

For wires with (110) and (−110) cross section, this set of $\mathbf{k}^*$ readily translates into $k_x^*=j_x(110)$; $k_y^*=j_y(-110)$ in units of $\frac{2\pi}{Na_0}$ where N is the number of atomic monolayers within the wire width L, a_0 is the bulk lattice constant, and j_x, j_y are integer quantum numbers.

B. Wave-function projections

To analyze the solutions of Eq. (1) in terms of the bulk states of Si, here we introduce a projection scheme in which we first (i) truncate the solutions of Eq. (1) at the wire boundaries, $x = 0$, L, and $y = 0, L$ (i.e., we ignore the tails outside $0< x,y < L$) and analytically continue the truncated wave functions into regions

of $-L < x < 0$ and $-L < y < 0$. We further require that the new wavefunctions, $\psi^*(\mathbf{r})$, defined now in the $-L < x < L, -L < y < L$ region, to be antisymmetric with respect to the $x = 0$ and $y = 0$ planes, i.e.,

$$\begin{aligned} \psi^*(\mathbf{r}) &= -\psi^*(-x, y, z) \quad \text{for } -L < x < 0, \\ \psi^*(\mathbf{r}) &= -\psi^*(x, -y, z) \quad \text{for } -L < y < 0, \\ \psi^*(\mathbf{r}) &= \psi^*(-x, -y, z) \quad \text{for } -L < x, y < 0. \end{aligned} \tag{8}$$

This antisymmetric continuation of the wave functions is a reasonable choice here since, other than the surface states for which no projection is attempted, all bulk-like wire states approach zero quickly, thus establishing nodes at the boundaries upon continuation. An example here is the EMA solutions to the quantum wires [Eq. (4)] where since the periodic function, $u_{n,\mathbf{k}_0}$, is assumed to be none vanishing at the boundaries, the envelope functions $\phi = C \sin(j_x \pi / Lx) \sin(j_y \pi / Ly)$ [see Eq. (7)] must, and in fact, satisfy Eq. (8). However, by allowing the total wave function of Eq. (1), not just the envelope function ϕ, to fulfill Eq. (8), we are not bounded by the EMA approximation in the current projection scheme. For example, it will pick up states with novel cosinelike envelope functions and vanishing $u_{n,\mathbf{k}_0}$ at the boundaries. As we have demonstrated in our earlier work,[13] such states do exist and are important in Si quantum films. (ii) In the second step, we make $\psi^*(\mathrm{r})$ periodic over the entire $\mathbf{r}$ space and project them onto a discrete set (in the x-y plane) of bulk states,

$$\begin{aligned} \{\chi_1 &= u_{n,k_x^*,k_y^*,0} e^{i(k_x^* x + k_y^* y)}, \\ \chi_2 &= u_{n,k_x^*,k_y^*,0} e^{i(-k_x^* x + k_y^* y)}, \\ \chi_3 &= u_{n,k_x^*,k_y^*,0} e^{i(k_x^* x - k_y^* y)}, \\ \chi_4 &= u_{n,k_x^*,k_y^*,0} e^{-i(k_x^* x + k_y^* y)}\}, \end{aligned} \tag{9}$$

where $\mathbf{k}^*$ are given by Eq. (5), the same EMA quantization conditions. This set of states forms a complete and orthogonal basis for any function periodic over $-L < x, y < L$. In this way, we are able to use the projection

$$|a_{n,f}(\mathbf{k}^*)|^2 = \sum_{i=1,4} |\langle \psi_f^{\text{wire}}(\mathbf{r}) | \chi_i(\mathbf{r}, \mathbf{k}^*) \rangle|^2 \tag{10}$$

to determine the identity of the directly calculated wire states in terms of their bulk parentage states. It is worth to mention here that the bulk projection scheme needs not be unique. For example, Hybertsen[20] for a different purpose had projected his quantum box states onto a bulk continuum. The EMA results in his scheme thus are represented by a broad peak in the reciprocal space whereas in the present scheme where the standing wave solution is already factored in, in the limit that $L \longrightarrow \infty$, they are, instead, simple single δ-functions.

IV. RESULTS

A. Free-surface wires

Table I summarizes the projections [Eq. (10)] of the directly calculated wire states for an 8×8 Si wire with a free surface and H-covered wire onto the bulk Si wave functions. We label the wire states as follows: First, wire states are designated by running index f starting at the valence-band minimum. Hence, f=112 is the VBM for the free-surface wire and f=144 is the VBM for H-covered wire. Second, it is sometimes convenient to use the label $V-1$, $V-2$, etc., to designate states below the VBM. Table I provides a "dictionary" between the two sets of nomenclatures.

Table I shows that free-surface wire states have more than 93% projections on bulk Si wave functions for the two lowest valence bands ($n = 1$ and $n = 2$) in the energy range from $E_v(\equiv E_{\text{VBM}}) - 11.7$ to $E_v - 3.3$ eV.

The situation changes somewhat when higher-energy wire states derived from the upper $n = 3, 4$ bulk bands are considered. Table I shows that the directly calculated states within 1 eV below the VBM (between f=107 and f=112) sometimes exhibit smaller projections of $\sim 80\%$, thus more than one bulk state (n, k) are involved in these states probably due to the presence of surface states.

B. Hydrogen-covered wires

Hydrogen chemisorption displaces the gap states into the continuum (Fig. 4) thus also perturbing the Si states. The lower part of Table I gives the projections of Eq. (10) for the H-covered wire states near the VBM, while Fig. 5 shows their wave-function amplitudes for the 8×8 case of both free-surface and hydrogen-covered wires. We see that H chemisorption leads to important changes as follows: *In the presence of H coverage*, the VBM has wave-function amplitude concentrated more in the *interior* of the wire while *without hydrogen*, the VBM has its wave-function amplitude concentrated in the *exterior* of the wire. In either cases, the VBM is nearly a pure n=3,4 bulk state ($\geq$90% projection) showing that it is not a surface state. The next state below the VBM for the H-covered wire ($V-1$) is a singlet, with the amplitude localized at the center of the wire. In contrast, in the wire without hydrogen, the $V-1$ state is a doublet with the wave-function amplitude localized at the *exterior* of the wire [Fig. 5(a)]. To identify the symmetry features of the near-gap states, we introduce here another set of labels, i.e., vs and cs for valence- and conduction-band singlets, and vd and cd for valence- and conduction-band doublets, respectively. These are used in Fig. 5(b) for the H-covered wire. In general, *hydrogen chemisorption enhances the localization of the near-band-edge wire states in the interior of the wire, thus making them reflect the Si skeleton.*

Previous theoretical calculations on Si wires[7,8,10] consider only H-covered wire surface. Figure 6 compares our calculated band gaps with other theoretical results for this case. The agreement with TB is excellent. The agreement with the LDA calculations (including band-gap corrections) is reasonable for the wire size larger than 6×6 monolayers, but for the 4×4 wire where all the atoms are either surfacelike or subsurfacelike, the LDA gives a gap that is about 0.8 eV smaller than the present results. We are aware that our approach is more adequate for

wires of larger sizes. The experimental band gaps range from 1.6 to 2.5 eV but the wire size is not accurately determined.

C. Effective mass vs direct calculations

To assess the validity of the commonly used EMA, we plot in Fig. 7 (last column) the EMA wave functions of Eq. (7) for the $j_x=j_y=1$ band-edge states. The corresponding states of the direct calculations for the free-surface wire and H-covered wire are shown in Fig. 7 as the first and second column, respectively. From Fig. 7, it is clear that the EMA approach bears no similarities to the direct calculations (free-surface and H-covered surface alike) for several valence-band-edge states (n=2 and n=4 in Fig. 7). This is because in the EMA, all envelope functions are sinelike, peaking at the center of the wire whereas the true wave functions, as revealed by the direct calculations, are hollow in the wire center, instead. The $n = 5$ conduction-band-edge states are composed of two distinct $j_x=j_y$ states (cs1 and cs2). In the free-surface wire, cs2 is below cs1 but the order is reversed in H-covered wire. In contrast, the EMA approach cannot tell the difference between the two (one of them is, therefore, lost).

D. Relative role of quantum confinement and surface chemisorption effects on wire band gaps

Figure 8 shows the band gap as a function of the wire size from our two model wire calculations and EMA.[7] All three have larger band gaps as wire sizes get smaller. Quantum confinement effects thus play an important role here. Compared with direct calculations, however, EMA overestimates the band-gap opening. Hydrogen

TABLE I. Projection squares [Eq. (10)] of the directly calculated wire states for the 8×8 Si wire with a free surface (upper part) and for the H-covered wire (lower part). The labels $V - i$ $(C + i)$ denote the ith wire state below (above) the corresponding VBM (CBM). For the free-surface wire the VBM is f=112, while for the H-covered surface VBM is f=141.

Wire energy (eV)	Wire state index f	Bulk band index n	Allowed $k = \frac{\pi}{L}(j_x, j_y)$ Eq. (5)	Projections (%) $\lvert a_{n,f}(k_x, k_y)\rvert^2$ Eq. (10)
		Wire with free surface		
−11.71	1	1	(1,1)	99.8
−11.25	2	1	(1,2)	99.5
−11.25	3	1	(2,1)	99.5
−10.83	4	1	(2,2)	99.3
−10.56	5	1	(1,3)	98.2
−10.56	6	1	(3,1)	98.2
−10.14	7	1	(2,4)	97.9
−10.14	8	1	(4,2)	97.9
−9.72	9	1	(4,1)	93.7
−9.72	10	1	(1,4)	93.7
−9.45	11	1	(3,3)	98.3
−7.68	22	2	(4,4)	98.3
−5.61	45	2	(3,3)	97.3
−3.32	60	2	(2,2)	93.3
−0.97	103	2	(1,1)	94.0
−0.36	109 (V−2)	3	(1,1)	80.7
−0.32	110 (V−1)	3, 4	(1,2)	76.7
−0.32	111 (V−1)	3, 4	(2,1)	76.7
0.0	112 (VBM)	4	(1,1)	92.1
		H-covered wire		
−.19	140 (V−3)	2	(1,1)	81.8
−.035	141 (V−2)	2, 3, 4	(1,1)	84.5
−.035	142 (V−2)	2, 3, 4	(1,1)	84.5
−.022	143 (V−1)	3, 4	(1,1)	93.3
0.00	144 (VBM)	3, 4	(1,1)	90.1
2.32	145 (CBM)	5,6	(3,3)	77.5
2.34	146 (C+1)	5,6	(3,3)	74.3
2.34	147 (C+2)	5,6	(3,3)	75.3
2.34	148 (C+2)	5,6	(3,3)	75.3

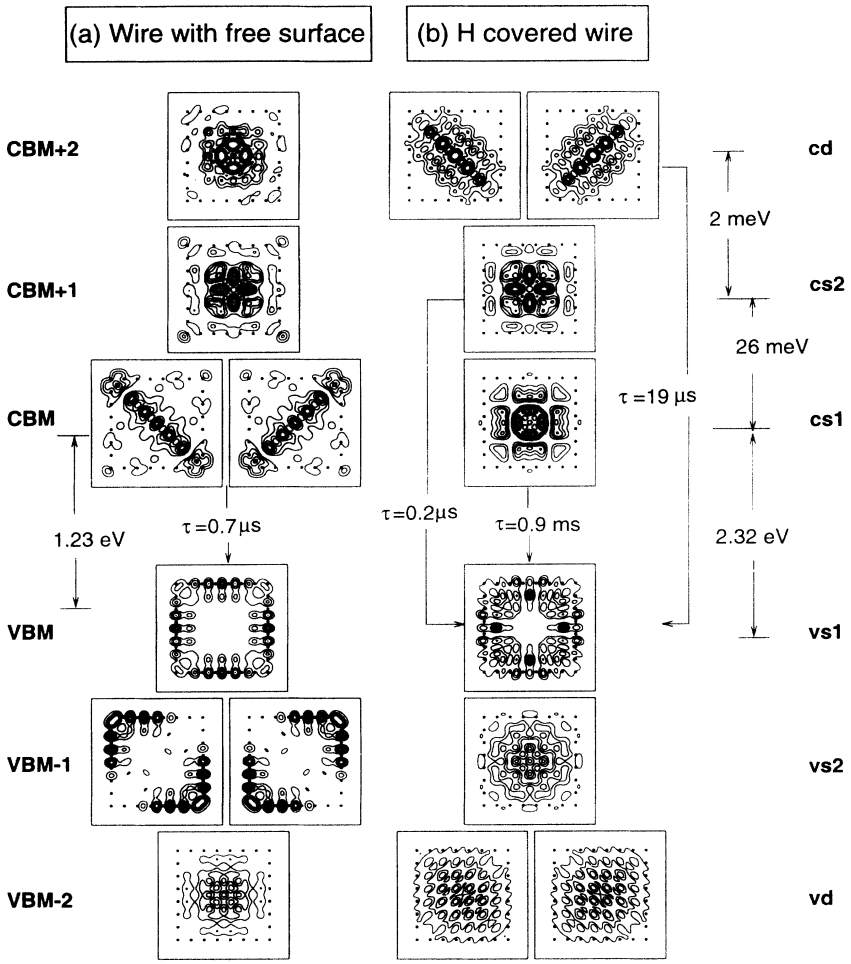

FIG. 5. Near-valence-band maximum z-direction averaged wave function square for an 8×8 Si wire: (a) wire with free surface and (b) hydrogen covered Si wire. Energy separations and radiative lifetimes are also shown. The dots denote the positions of the outermost Si atoms. The states of the H-covered wire are also labeled as "vs1"= 1st valence singlet; "vs2"=2nd valence singlet; "vd"=valence doublet; "cs1"= 1st conduction singlet, etc.

chemisorption effects act to *reduce* the band gap of the free-surface wires, because adding H atoms on Si free surface removes the surface states from the gap and effectively enlarges the size of the wires.

E. The nature of the near-gap electronic states in hydrogen covered wires

Having discussed our directly calculated results and compared them to those obtained with previous direct calculations, and with the effective-mass method (Sec. IV A–C), we now focus on a more detailed discussion of the electronic structure of hydrogen covered wires.

Figure 9 shows the near-gap energy levels of hydrogen-covered wires in the size range of 6×6 to 12×12. This figure also gives the interband gap as well as the exciton-corrected gap (in parenthesis). The correction was taken from Ref. 10 which considers a similar range of wire sizes to what is calculated here. However, Ref. 10 used dielectric constant of bulk Si, thus underestimating the exciton binding energy. Ohno *et al.*[9] considered the effects of the surrounding material on ultrathin Si wires (3×3 to 5×5). They find an additional 0.12 eV exciton reduction in the gap for a 4×4 wire. Such effects, however, reduce as the wire width increases.

It is characteristic of the wires we studied that near the top of the valence band there are two singly degenerate levels, vs1 and vs2, as well as a doubly-degenerate level, vd. The energy spread of the four levels is within 0.06 eV. Similarly, the conduction-band minimum consists of two singly degenerate states, cs1 and cs2, as well as a doubly degenerate state, cd. Again, the energy spread is only 0.05 eV. Other zone center energy levels are well-separated from these four valence and four conduction levels (as can be seen from Fig. 9). Thus, the near-threshold optical properties can be discussed considering only these levels. Figure 5(b) depicts the characteristic wave-function-square pattern of these near-edge levels. While the *order* of the four valence (or four conduction) levels can change with wire size, their characteristic patterns remain fixed, as shown in Fig. 10. Note that the wave functions can be classified according to their parity with respect to mirror plane reflection, the singlet state is polarized in the z direction and the doublet is polarized in the x and y directions.

It is interesting to characterize these levels by radiative lifetimes, and by dipole matrix elements. The matrix element for direct transitions coupling states (i) and (f)

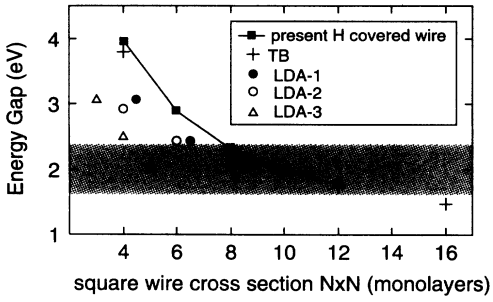

FIG. 6. Band gaps (without exciton corrections) of hydrogen-covered Si wires vs size as given by different calculations. TB is the tight-binding result of Ref. 10 , LDA-1 is from Ref. 7, LDA-2 is from Ref. 8, and LDA-3 is from Ref. 9. The present results are indicated by filled squares. The experimental band gaps tend to cover a broad area denoted by the shading.

is given by

$$M_{if} = \langle \psi_i | \mathbf{p} | \psi_f \rangle = -i \int \psi_i^*(\mathbf{r}) \nabla \psi_f(\mathbf{r}) d^3r \quad . \tag{11}$$

Here, $\mathbf{p} = -i\nabla$ is a momentum operator. The radiative lifetime is calculated[21] by

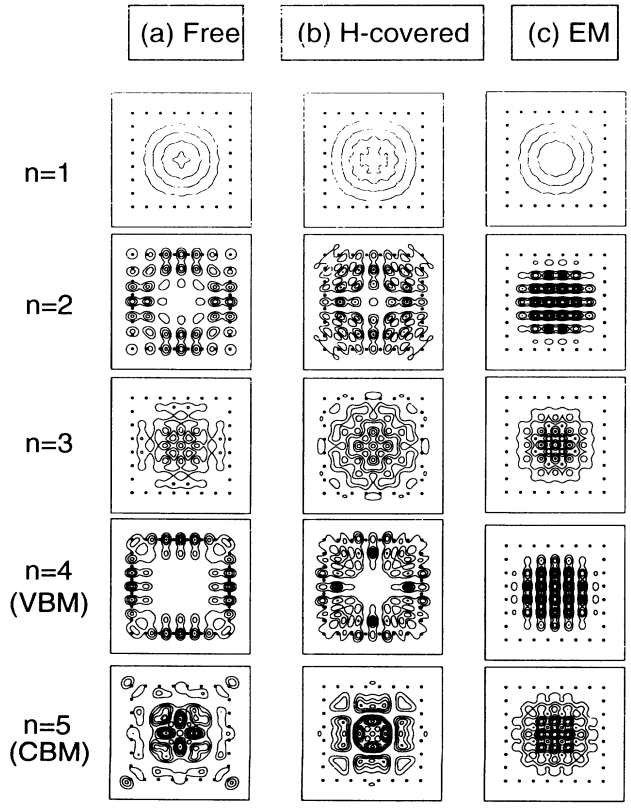

FIG. 7. Comparison of the z-direction averaged wave function squares for an 8×8 Si wire. (a) Directly calculated (Dir) free surface wire, (b) directly calculated H-covered wire, and (c) effective-mass wire. The dots denote the positions of the outermost Si atoms.

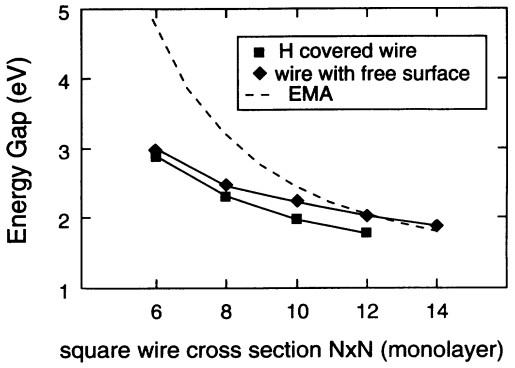

FIG. 8. Band gaps (without exciton correction) between intrinsic states in Si wire as a function of size.

$$\frac{1}{\tau_R} = \frac{4\alpha\,\omega\,n}{3m_e^2\,c^2}|M_{if}|^2, \tag{12}$$

where α is the fine structure constant, ω is the photon angular frequency, n=1.48 is the experimental[22] refractive index of porous Si, m_e is the free electron mass, and c is the velocity of light. We used EPM together with Eq. (12) to calculate τ_R for the direct gap in GaAs and found τ_R=0.79 nsec, compared with the measured value[23] τ_R=1 nsec. Figure 5 gives the calculated radiative lifetime for the near-gap states in the 8×8 Si wire (part a) without and (part b) with hydrogen.

Figure 11 depicts the energy dependence of the radiative lifetimes of all zone center level pairs starting from the upper four valence levels and continuing into the conduction band. It applies to the emission processes where transitions are confined largely to the zone center. Besides the blueshift of the spectral threshold, we notice that the τ_R vs ϵ spectra consists of well-defined bands denoted as α, β, and γ. Band α consists of the

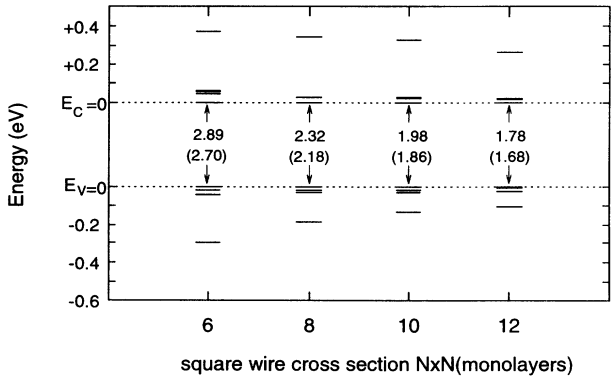

FIG. 9. Energy levels of H-covered Si square wires with cross section ranging from 6×6 to 12×12. Only the five lowest energy states of the conduction band and the five highest energy states of the valence band are shown in the figure. Band gaps without and with excitonic correction (in parentheses) are given. The excitonic shift is taken from Ref. 10. The energies are measured from E_v (VBM) and E_c (CBM), respectively.

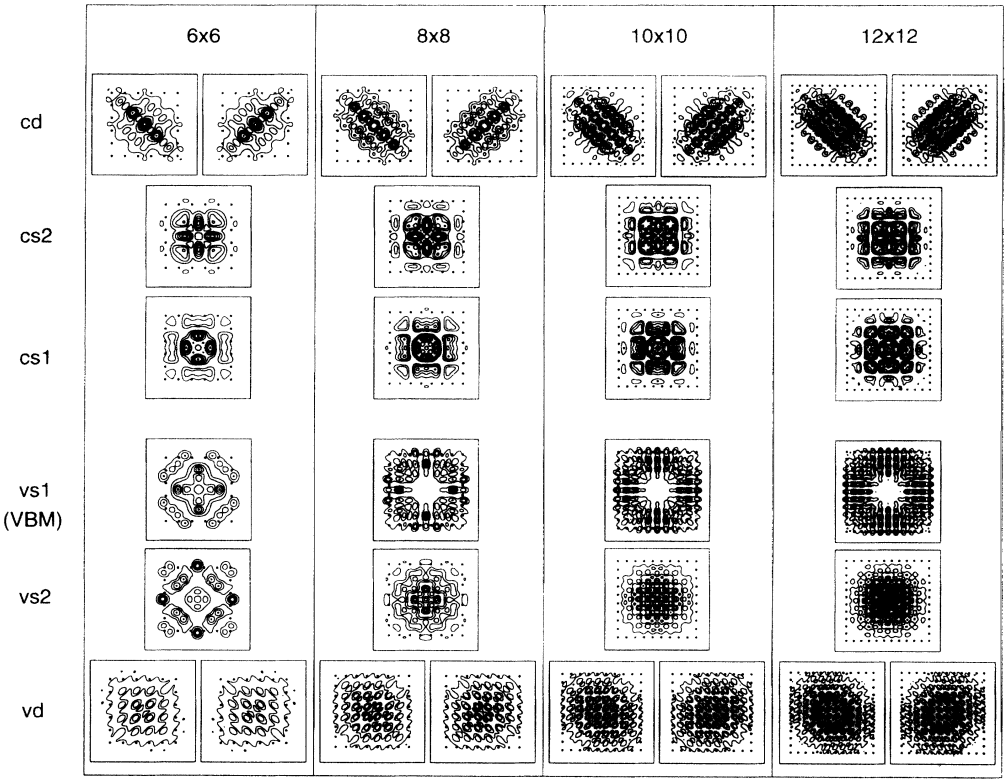

FIG. 10. z-direction averaged wave function square for the near-gap states in various H-covered Si wires.

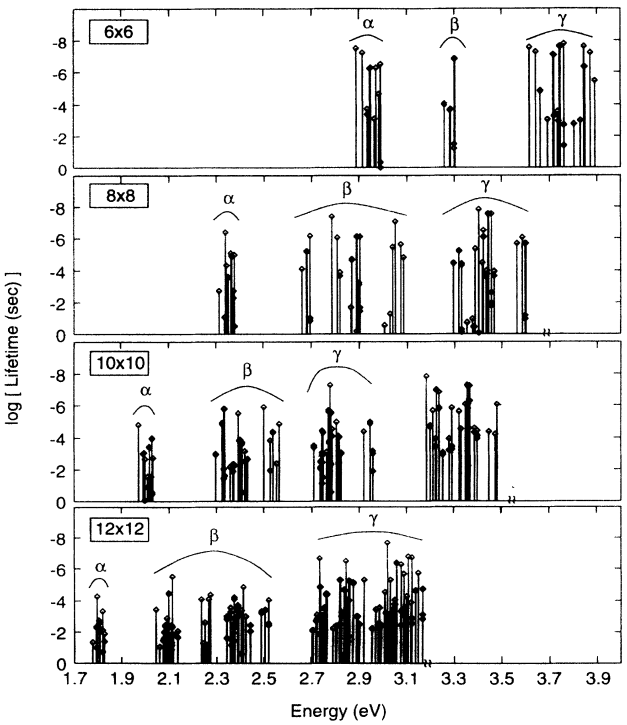

FIG. 11. Calculated radiative transition lifetime from the four highest valence-band states as a function of the transition energy (no excitonic correction).

16 transitions coupling the four lower conduction-band states with the four upper valence-band states; bands β represent transitions from the higher-energy conduction states to the upper four valence states, etc. Each band is seen to contain very slow (i.e., nearly dipole forbidden or $\tau_R > 10^{-3}$ sec) as well as faster transitions. Calcott *et al.* interpreted their "very slow" transitions (see Fig. 1) as resulting from spin triplets. Although our calculations are spin-restricted, they do indicate, however, that nearly forbidden very slow transitions exist at threshold

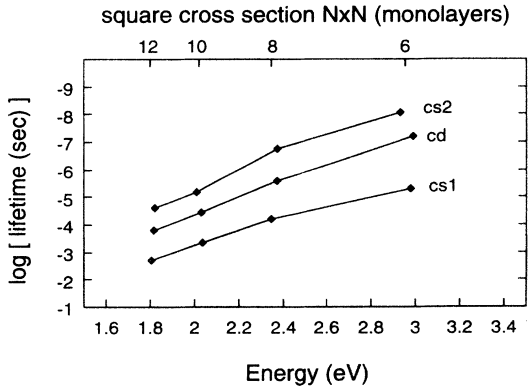

FIG. 12. Calculated energy dependence of the radiative lifetime for the cs1, cs2, and cd conduction states to the four highest valence states.

just due to orbital (not spin) symmetry. Figure 12 shows that the prototype conduction-band states cs1, cs2, and cd depicted in Fig. 10 have distinct lifetimes connecting each of them to the four topmost valence-band states. Thus, the prototype wave-function *shapes* of Fig. 10 represent also prototype *radiative lifetimes* in Fig. 12.

In the present study, the band edge transition lifetime from cs1 to vs1 is 9×10^{-4} sec for an 8×8 wire. It compares with 6.94×10^{-5} sec from conduction-band maximum (CBM) to VBM of Sander and Chang *et al.*[10] and differs by one order of magnitude. The symmetries of the band-edge states in our calculation are, however, different from Sander's. As we have demonstrated earlier in Sec. III, these symmetry properties may vary, due to the narrow spread of these states, when different H potentials are used. Given this fact, it is probably meaningful only to compare the most probable transitions in this group (or band). We, therefore, calculate $\tau_{\rm band}$ where $\frac{1}{\tau_{\rm band}} = \sum_i^N \sum_f^N \frac{1}{\tau_{if}}$. Without occupation average, this expression gives a measure of the overall strength of the optical transitions in each band. With this modification, our $\tau_{\rm band} = 1.5\times10^{-7}$ sec compares reasonably well with that of Sander's (8.3×10^{-7} sec). Read *et al.*[7] did not report the necessary information to calculated $\tau_{\rm band}$ so a direct comparison is not possible. Their band threshold transition lifetime is 3.8×10^{-4} sec for an 8×9 wire which is closed to our result for a 8×8 wire (9×10^{-4} sec). In Fig. 13, we plotted $\tau_{\rm band}$ also for the β, γ bands for which the energy spread is, however, much larger (Fig. 11). It shows that the transition lifetimes decrease exponentially with the wire size. The lower-energy band α has a slower decay than the higher energy bands β and γ. This "slow" or "weakly allowed" transition reflects the pseudodirect nature of the wire band gap and is associated here with the conventional S-band red emission from porous Si. The "fast" transitions β and γ, on the other hand, obtain their spectral weight from the higher energy *direct* transitions in bulk Si, as demonstrated earlier.[13] These transitions, nevertheless, do not occur at threshold (see Fig. 11).

F. Quantum wire vs quantum box states

Our discussion has focused thus far on wires with a [110]-[$\bar{1}$10] cross section and length $L_z \to \infty$. However, experimentally made porous Si can include not only a distribution of x-y cross sections (denoted by $N\times N$), but also *finite* lengths L_z. The near-gap electronic structure (α band) of quantum boxes with the same cross section as our wire calculation ($L_x{=}L_y{=}\frac{1}{\sqrt{2}}L_z$) has been calculated recently by Wang and Zunger[16] using precisely the same pseudopotentials and atomic geometries. The calculated band gaps and lifetimes are compared with Si wires in Fig. 14. As expected, given the same lateral (x-y) cross section, the band gap of the box is larger than that of the wire due to the additional (finite L_z) confinement in the box. However, the radiative lifetime of the box is seen (on a logarithmic scale) to be only slightly longer than that of the wire. Thus, despite a greater confinement, transitions in the box are "less" allowed (reflecting a smaller overlap of wave functions in the z direction) than in wire.

This should be contrasted with the behavior shown in Fig. 13, namely that changing the *size* of a wire with a fixed shape leads to a (nearly exponential) change in the radiative lifetime, yet changing a wire into a box (Fig. 14) leaves the lifetime essentially unchanged while strongly affecting its band gap.

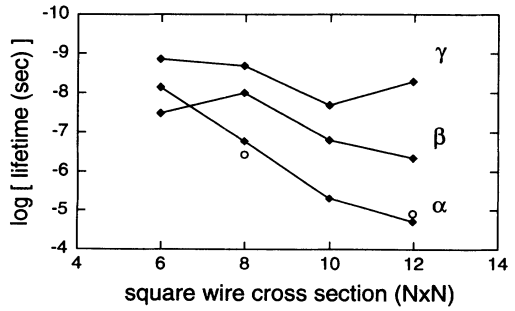

FIG. 13. Transition lifetime connecting the four highest valence states to bands α, β, and γ shown in Fig. 11. Open circles denote the TB result of Ref. 10.

V. DISCUSSIONS AND CONCLUSIONS

We have examined the (i) quantum confinement effects and (ii) surface chemisorption effects on the electronic structure of (001) Si wires. Our results can be summarized as follows:

(i) Near the VBM the main contribution to the wire states comes from the two highest valence bands at a single off-Γ k vector, $\mathbf{k}$. Similarly, the wire CBM is formed predominantly from the lowest bulk conduction band at a single $\mathbf{k}$, e.g., at $j_x{=}j_y{=}3$ for an 8×8 wire (Table I). Hence, it is still meaningful to discuss wire transitions in bulk terms. In particular, the transition connecting

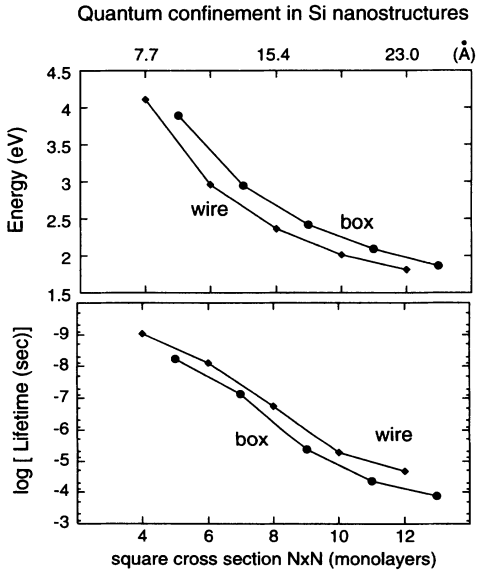

FIG. 14. Comparison of the α band radiative lifetime and the band gap of quantum wires with quantum boxes.

the band edge states in a wire are pseudodirect, not direct. This is reflected, among others, by the logarithmic change in lifetime with size (Fig. 13) .

(ii) Since the wire states are formed from off-Γ states (for the VBM) and off-Δ_c states (for the CBM), the nonparabolicity of the bulk bands away from these band edges becomes important, especially for narrow wires. Furthermore, the wire state may consist of multiband coupling (Table I) and involve non-effective-mass cosine-type envelope function. Not surprisingly, simple effective-mass models cannot describe well such complicated situations regardless whether H coverage is included or not (Fig. 7).

(iii) The effects of hydrogen chemisorption are seen in two aspects. First, the level ordering may change: the CBM xy-polarized, doubly degenerate states with $j_x \neq j_y$ change order with the z-polarized, singly degenerate $j_x = j_y$ state in Fig. 5. Second, the wave-function localization may change: near the band edge, wave functions localized at the *exterior* of the wire are transformed into states with wave-function localization more at the *interior* of the wire (e.g., the VBM in Fig. 5). Thus, after chemisorption the near-band-edge states reflect more closely the properties of the Si skeleton of the wire rather than its outer layers. This implies that as long as *all* dangling bonds are passivated, the value of the band gap will probably not depend sensitively on the type of passivant (e.g., H or oxygen).

(iv) Both free-surface wire and H-covered wire have sizeable blueshifts in the band gap. This means that quantum confinement effects play an important role. The net effect of surface chemisorption is to increase the gap by a small fraction. Unfortunately, the significant distribution of wire sizes, which exists in currently made samples, leads to a concomitant wide distribution of emission energies. It is thus not possible to determine at present if a quantitative agreement exists between experiment and confinement-based theories.

(v) The near-gap zone center states in the wire appear as four closely spaced valence and four closely spaced conduction levels (Fig. 9). They have distinct wave-function patterns (Fig. 10) and lifetimes (Fig. 12). The overall lifetime vs energy spectrum near the zone center (Fig. 11) shows well-defined bands. The lowest energy band (α, or "slow") has the longest decay time, while the higher energy band (β, or "fast") couples better with the direct bulk bands for $N > 6$ and have thus a shorter radiative lifetime (Fig. 13).

(vi) Quantum boxes have larger band gaps but comparable radiative lifetimes to wires of the same lateral geometry (Fig. 14).

It is tempting to compare our theoretical results on quantum wires and boxes to the experimental data on *porous* Si. The comparison is, however, problematic given that *porous* Si appears to represent a *distributions* of (a) wire *sizes* (i.e., different $N_x; N_y$), (b) *lengths* (i.e., "wires" with large N_z vs boxes), (c) shapes, (d) surface orientations, and (e) surface terminations. In fact, the PL experiments of Calcott *et al.*[5] pertain to wires of an average cross section of 30±10 Å; this wide size distribution translates into a distribution of ±0.6 eV in *band gaps*, so a compelling comparison of measured and calculated band gap values is not possible at present (the measured S-band *peak* position of 1.76 eV agrees with our calculated results for a 12×12 wire with a gap energy 1.77 eV). Likewise, the 0.4 eV *width* of the S-band PL (1.7 to 2.3 eV) is indicative of a possibly wide distribution of sizes and shapes. Indeed Fig. 11 indicates that if one has good *energy* resolution but no *size* resolution then the emissions in the range of 1.7 to 2.3 eV can be expected to come anywhere from 8×8, 10×10, and 12×12 wires and from comparable quantum boxes (Fig. 14). Thus, a *detailed* comparison with theory must await the synthesis and characterization of size, shape, and surface *controlled*, mono-dispersed Si quantum structures. In the interim one could make the following remarks:

(i) The lifetime (weighted by all possible transitions in the α band) vs energy curve of the wires (Fig. 15) agree qualitatively with the similar plot of Calcott *et al.*[5] for their S band and other experimental data.[24,25] However, the calculated curve shows a faster increase of τ_R with size compared with the measured curve. This means that as size increases the calculated α-band transitions become nearly forbidden faster than the measured S band does.

Similar is true for the α band in the quantum *boxes*.

(ii) As Fig. 14 illustrates, a wire and a box having the same lateral dimension will have approximately the same τ_R but significantly different band gaps. This means that by assuming that a sample is made of wires *and* boxes, the slope of the τ_R vs ϵ curve can be made arbitrarily flat. This could explain the fact that Calcott's data has a significantly smaller slope than the results for *pure* wires. In fact, it is reasonable to imagine that at the beginning of the etching process of porous Si one forms mostly *thick* wires, while after extended etching the wires thin down into *linked-sausage shapes*.[26] The necks of the linked sausage provide the third dimension confinement. Once the confinement effects is large enough, the wires effectively break into *quantum boxes*. Thus, the small photon energy region should represent mostly emission from wires while the higher photon energy region could

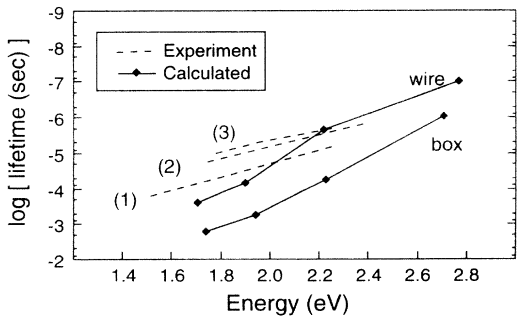

FIG. 15. Comparison of the calculated lifetimes (weighted by all possible transitions, τ=16τ_{band}) of quantum wires and quantum boxes with experimental results. Data (1) [Ref. 24], (2) [Ref. 25], and (3) [Ref. 5] are for the S band in porous Si. The calculated results include excitonic energy corrections (Ref. 10).

represent a larger contribution from boxes. This means that the "effective" τ_R vs ϵ curve should consists of the wire contribution at small ϵ, moving into a box contribution at larger ϵ. This is a flatter curve than for pure wires or boxes.

(iii) A β-band transition of the 8×8 wire in the energy range of 2.8 eV (without excitonic reduction) appears to have a lifetime of 8.5 nsec, in line with the measured F-band transition from about 10 to 100 nsec in porous Si. A more definitive conclusion, however, requires the energy dependence of the lifetime also being measured and an understanding of the competing nonradiative decay through other channels (defects, dangling bonds, etc.).[27]

ACKNOWLEDGMENTS

We would like to thank L. W. Wang and S. Froyen for many helpful discussions. This work was supported by the Office of Energy Research (OER) [Division of Materials Science of the Office of Basic Energy Science (BES)], U.S. Department of Energy, under Contract No. DE-AC02-83-CH10093.

[1] L. T. Canham, Appl. Phys. Lett. **57**, 1046 (1990).

[2] See many articles on porous Si in *Light Emission from Silicon*, edited by S. S. Iyer, R. T. Collins, and L. T. Canham, MRS Symposia Proceedings No. 256 (Materials Research Society, Pittsburgh, 1991), and in *Microcrystalline Semiconductors: Materials Science and Devices*, edited by P. M. Fauchet, C. C. Tsai, L. T. Canham, I. Shimizu and Y. Aoyagi, MRS Symposia Proceedings No. 283 (Materials Research Society, Pittsburgh, 1993).

[3] A. V. Andrianov, D. I. Kovalev, V. B. Shuman, and I. D. Yaroshetskii, Pis'ma Zh. Eksp. Teor. Fiz. **56**, 242 (1992) [JETP Lett. **56**, 236 (1992)].

[4] V. Petrova-Koch, T. Muschik, A. Kux, B. K. Meyer, F. Koch, and V. Lehmann, in *Microcrystalline Semiconductors: Material Science and Devices* (Ref. 2), p. 179.

[5] P. D. J. Calcott, K. J. Nash, L. T. Canham, M. J. Kane and D. Brumhead, J. Physics. Condens. Matter **5**, L91-L98 (1993).

[6] This temperature is taken from Ref. 4. However, Cullis *et al.* found in their samples that the intensity of the S band is strongest at 950 °C and decreases at above 1000 °C (p. 257 of Ref. 4).

[7] A. J. Read, R. J. Needs, K. J. Nash, L. T. Canham, P. D. J. Calcott, and A. Qteish, Phys. Rev. Lett. **69**, 1232 (1992); *ibid.* **70**, 12 050 (1993).

[8] F. Buda, J. Kohanoff, and M. Parrinello, Phys. Rev. Lett. **69**, 1272 (1992).

[9] T. Ohno, K. Shiraishi, and T. Ogawa, Phys. Rev. Lett. **69**, 2400 (1992).

[10] G. D. Sanders and Y. C. Chang, Phys. Rev. B **45**, 9202 (1992); J.-B. Xia and Y. C. Chang, *ibid.* **48**, 5179 (1993).

[11] M. Hybertsen and M. Needels, Phys. Rev. B **48**, 4608, (1993).

[12] There is a misprint of 2.24 Å in an earlier publication on this subject: C.-Y. Yeh, S. B. Zhang, and A. Zunger, Appl. Phys. Lett. **63**, 3453 (1993).

[13] S. B. Zhang, C.-Y. Yeh, and A. Zunger, Phys. Rev. B **48**, 11 204 (1993).

[14] J. R. Chelikowsky and M. L. Cohen, Phys. Rev. B **14**, 556 (1976).

[15] F. G. Allen, J. Phys. Chem. Solids **8**, 119 (1959).

[16] L. L. Wang and A. Zunger, J. Phys. Chem. **98**, 2158 (1994).

[17] The reciprocal-space form of H potential A is $V_H(g) = -65.83 + 62.70g - 15.78g^2 - 2.30g^3 + 1.00g^4$ when $g \leq 3.21$ and $V_H(g) = -19.60 + 11.50g - 2.85g^2 + 0.34g^3 - 0.0152g^4$ when $3.21 > g \leq 6.41$ and $V_H(g) = -6.13 + 1.74g - 0.185g^2 + 0.0086g^3 - 0.00015g^4$ when $g > 6.41$. Here, the reciprocal lattice vectors g are in atomic units and the potentials are in Ry.

[18] Z. Berkovitch-Yellin, D. E. Ellis, and M. A. Ratner, Chem. Phys. **62**, 21 (1981).

[19] V.I. Gavrilenko, P. Vogl and F. Koch, in *Microcrystalline Semiconductors: Material Science and Devices* (Ref. 2), p. 431.

[20] M. S. Hybertsen, in *Light Emission from Silicon* (Ref. 2), p. 179.

[21] C. H. Henry and K. Nassau, Phys. Rev. B **1**, 1628 (1970). Equation (2) in Ref. 12 should be mutiplied by a factor of 2.

[22] R. Tsu, L. Ioriatti, J. F. Harvey, H. Shen, and R. A. Lux, in *Microcrystalline Semiconductors: Material Science and Devices* (Ref. 2), p. 437.

[23] C. J. Hwang, Phys. Rev. B **8**, 646 (1973).

[24] A. Bsiesy, F. Gaspard, R. Herino, M. Ligeno, F. Muller, R. Romestain, and J. C. Vial (unpublished).

[25] Y. H. Xie, W. L. Wilson, F. M. Ross, J. A. Mucha, E. A. Fitzgeral, J. M. Macaulay, and T. D. Harris, J. Appl. Phys. **71**, 2403 (1992).

[26] A. G. Cullis and L. T. Canham [Nature **353**, 335 (1991)] suggested undulating wires based on their TEM data.

[27] The experimental origin of the F band is unclear. For example, it has been suggested that the F band is oxide related [J. C. Vial and I. Mihalcescu, *Proceedings of the NATO Workshop on Optical Properties of Low Dimensional Si Structures* (Publisher, City, 1993), p. 117].

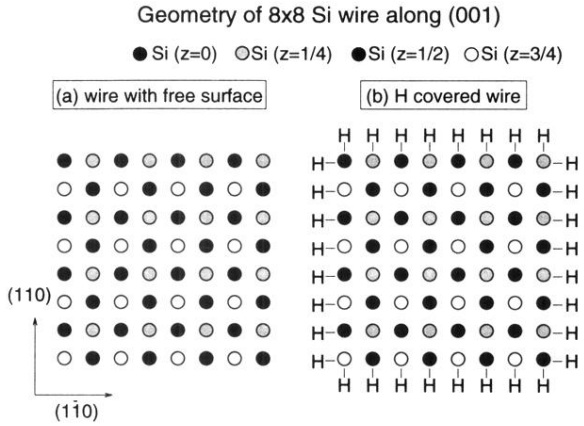

FIG. 3. Geometry of a (001)-oriented 8×8 Si wire with (110) × (1$\bar{1}$0) cross section, (a) free-surface wire and (b) hydrogen-covered wire.

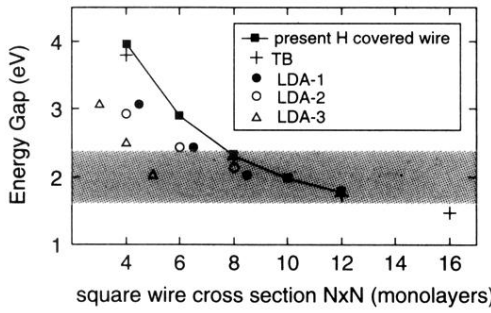

FIG. 6. Band gaps (without exciton corrections) of hydrogen-covered Si wires vs size as given by different calculations. TB is the tight-binding result of Ref. 10 , LDA-1 is from Ref. 7, LDA-2 is from Ref. 8, and LDA-3 is from Ref. 9. The present results are indicated by filled squares. The experimental band gaps tend to cover a broad area denoted by the shading.